Instability in pipe flow

D. L. Cotrell[†], G. B. McFadden[‡], and B. J. Alder[†§]

[†]Lawrence Livermore National Laboratory, Livermore, CA 94551; and [‡]Mathematical and Computational Sciences Division, National Institute of Standards and Technology, Gaithersburg, MD 20899-8910

The long-puzzling, unphysical result that linear stability analyses lead to no transition in pipe flow, even at infinite Reynolds number, is ascribed to the use of stick boundary conditions, because they ignore the amplitude variations associated with the roughness of the wall. Once that length scale is introduced (here, crudely, through a corrugated pipe), linear stability analyses lead to stable vortex formation at low Reynolds number above a finite amplitude of the corrugation and unsteady flow at a higher Reynolds number, where indications are that the vortex dislodges. Remarkably, extrapolation to infinite Reynolds number of both of these transitions leads to a finite and nearly identical value of the amplitude, implying that below this amplitude, the vortex cannot form because the wall is too smooth and, hence, stick boundary results prevail.

This work explores the effect of wall roughness on the long known contradiction between the linear stability analysis result of infinitely stable flow in pipes with smooth boundaries and the experimental observation (1) that flows become unstable at a Reynolds number of ≈2,000 for ordinary pipes (2–4). A hint that wall roughness may be important can be gathered from experiments which show that for smoothed pipes, the onset of the instability can greatly exceed 2,000 (5). The present work should serve as a general warning that stick boundary conditions—for example, in narrow biological channels where the surface roughness of the wall can be a significant fraction of the channel width, or, as another example, in the drag reduction problem—may be inappropriate. For the smooth-wall case, there exists a rigorous proof of stability for axisymmetric disturbances (6) and strong evidence (cf. refs. 7 and 8) that all linear perturbations decay for all values of the Reynolds number and axial and azimuthal wavenumbers. Thus, there remains much interest in the cause of this transition and how one may affect the Reynolds number at which transition occurs.

Most previous flow field calculations in modified channels (9–15) deal with heat and mass transfer augmentation, whereas stability calculations have mostly concentrated on flow between two infinite plates with varying cross-sections (16–21). In the recent linear stability work (21) for the modified parallel plate case, sinuous and square wave wall distortions are considered, with results showing that the base flow is significantly destabilized with respect to the smooth-wall case, and that the critical Reynolds number is only slightly affected by the shape of the wall distortions. However, as opposed to the pipe, the parallel plate configuration with constant cross-section leads to a finite Reynolds number instability. The primary focus of this work is to show that wall topography significantly alters the linear stability condition and to show that there may be a wall amplitude below which linear stability analysis gives results similar to those of the smooth-wall case. To date, the only previous linear stability work on wavy pipes is for a very restricted range of parameters (22) not including the small-amplitude case of interest here.

The flow of an isothermal constant property incompressible fluid in a corrugated pipe is governed by the Navier–Stokes equations (i.e., conservation of mass and linear momentum) which are made dimensionless by scaling the radial and axial directions by the mean radius ($\bar{R}$) and corrugation wavelength (Λ), respectively, while time, pressure, and velocity are scaled using the density (ρ), $\bar{R}$, and a characteristic axial velocity ($V_z =$

$[(\Gamma\nu)/(\beta\rho)]^{1/3}$), where Γ is the mean axial pressure gradient used to drive the flow, $\nu = \mu/\rho$ is the kinematic viscosity, μ is the dynamic viscosity, and $\beta = \bar{R}/\Lambda$ is the aspect ratio. A linear decomposition is used for the pressure $P(R, Z) = \hat{P}(R, Z) - \Gamma Z$, where $\hat{P}$ is axially periodic with the imposed corrugation wavelength. This decomposition has previously been used for the case of pressure-driven flow in a grooved channel and constricted pipe (12, 16, 22) and is consistent with axial periodicity of the velocity, as only the gradient of the pressure enters into the problem. The dimensionless wall radius is given by $r_w(z) = 1 - \varepsilon \cos(2\pi z)$, where ε is the dimensionless amplitude of the wall corrugation. Given the nondimensionalization above, the flow is driven by specifying the dimensionless mean axial pressure gradient $\Phi_z = [(\Gamma\Lambda\bar{R}^2)/(\rho\nu^2)]^{1/3}$.

The base flow is steady, axisymmetric, and axially periodic with the imposed corrugation wavelength and has no azimuthal velocity component. The boundary conditions are no slip on the pipe wall and boundedness at the centerline. The quadratically nonlinear system of differential equations governing the base flow is solved numerically using finite-element methods (23). A consistent penalty method is used to satisfy incompressibility, while quadrilateral elements (using an isoparametric mapping) with quadratic velocity and discontinuous linear pressure interpolation (cf. refs. 24 and 25) and 5 × 5 Gaussian quadrature are used for numerical integration. Discretization of the equations leads to a quadratically nonlinear algebraic system of equations which is solved by Newton iteration, where solutions at each Reynolds number are used as the initial iterate for the next highest value (i.e., zeroth order continuation). For regions of parameter space in which the use of zeroth order continuation is unable to converge to a solution, first order continuation (23) is used. To validate the base flow code, comparison was made to previous numerical results (9, 14, 15, 22), where authors have shown that the higher the wall corrugation amplitude, the earlier the vortex formation in the bulge region, that the vortex initially forms on the upstream portion of the bulge region, and that as the Reynolds number increases, the vortex core migrates toward the downstream boundary of the bulge region. These features of the base flow are consistent with the current results (see Fig. 1), and furthermore, the axisymmetric and axially invariant unidirectional solution of circular Poiseuille flow is recovered for the limiting case of no corrugation (i.e., $\varepsilon = 0$).

To investigate the linear stability of the base flow, a standard normal mode analysis (20, 21) is used which results in a system of homogeneous linear differential equations in the radial and axial coordinate for the velocity and pressure eigenfunctions. The disturbance velocity boundary conditions are zero on the pipe wall and again boundedness at the centerline. Since the coefficients of this system are 2π-periodic in the axial direction, Floquet theory (20, 21, 26) is used to consider disturbances whose structure is independent of the corrugation wavelength. Thus, in the computations, the velocity and pressure eigenfunctions have the form $\exp(\sigma t + ikZ + im\theta) f(R, Z)$, where $f(R,$
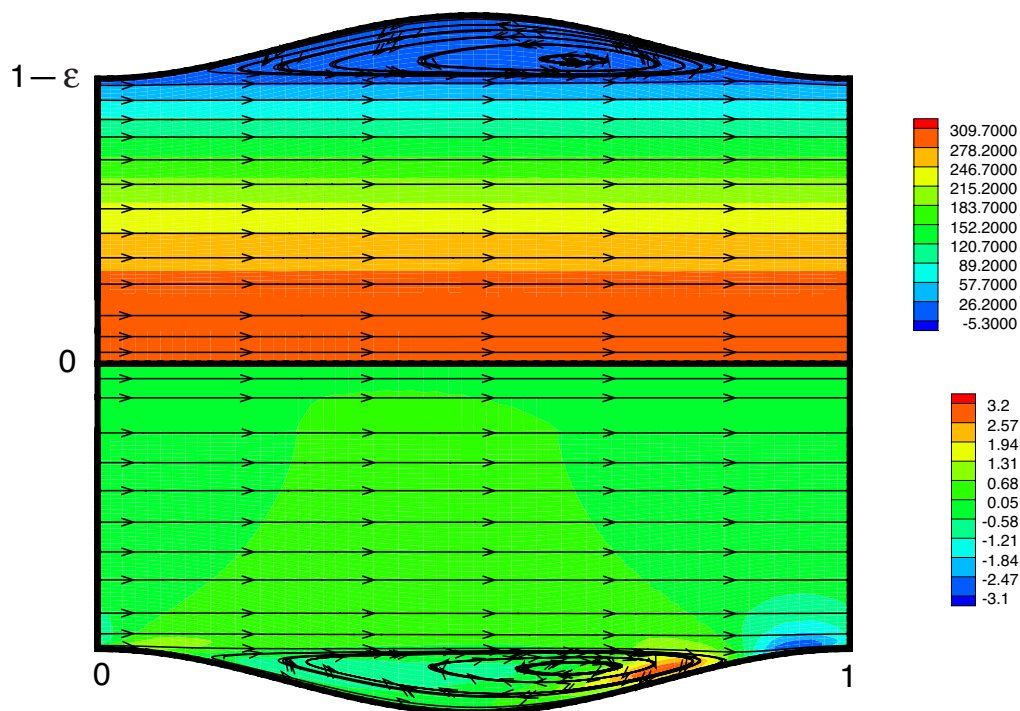
Fig. 1. Base flow velocity contours for $\beta = 1$, $\varepsilon = 0.1$, and $Re = 6{,}177$. The upper portion shows axial velocity shading and streamlines, while the lower portion shows radial velocity shading and streamlines.

Z) is 2π-periodic in Z, the temporal eigenvalue $\sigma = \sigma_r + i\sigma_i$ is complex, the disturbance axial wavenumber k is taken to be real, the azimuthal wavenumber m is taken to be an integer, and θ is the azimuthal coordinate. Discretization of the disturbance equations using finite-element methods (see the above base flow discussion) leads to a sparse generalized algebraic eigenvalue problem, where for fixed β, ε, and m a minimum Reynolds number is sought for which at least one temporal eigenvalue has $\sigma_r = 0$ for some k, and all other values of σ lie in the left half-plane for all k. The analysis is restricted to positive m and k without loss of generality, while the method used to locate critical values has been validated in previous work (27).

The current results of flow in a wavy pipe driven by an axial pressure gradient are given in terms of the aspect ratio (β) which is used to vary the corrugation wavelength, the corrugation amplitude (ε), and a Reynolds number [$Re = (\bar{V}_z \bar{R})/\nu$] based on the mean pipe radius and the mean axial velocity evaluated at the wall corrugation minimum (i.e., $z = 0$). The case of $\beta = 1$ is considered for simplicity, and a cursory investigation into the effects of nonaxisymmetric disturbances is performed to show that in the limit of small ε, only $m = 0$ (i.e., axisymmetric disturbances) needs to be considered.

For this case, results show that for fixed ε and small Re, the base flow is primarily unidirectional with significant streamline curvature seen only near the bulge and no vortex present in the domain (as opposed to the higher Re results shown in Fig. 1). As shown by the dashed curve in Fig. 2, for sufficiently large Reynolds number, the onset of vortex formation is observed in the bulge region; however, the flow is stable according to linear stability analysis both above and below this Reynolds number. There are various methods available to decide when a vortex is present (cf. ref. 28); however, only the simplest method available—namely, looking for negative axial velocity in the bulge region—has been employed. Because this method is slightly grid-dependent and one must set a threshold value (ideally set to machine precision but in the current study set to 10^{-10}), grid convergence studies have been performed for each geometry in

an attempt to get fairly grid-independent values. Although separation in the bulge region is not the primary focus of the present work, results seem to suggest the existence of a critical amplitude below which no vortex forms in the bulge region. If the Reynolds number is increased beyond this first transition, a value of Re is reached at which the steady and axisymmetric bulge vortex flow transitions to an unsteady flow ($\sigma_i \neq 0$) with different axial wavenumber than the wall corrugation wavenumber of 2π as shown in Fig. 3. There are no critical disturbances for which $k = 0$; however, for large enough corrugation amplitude, there is a value of Re for which the base flow becomes unstable to $k =$
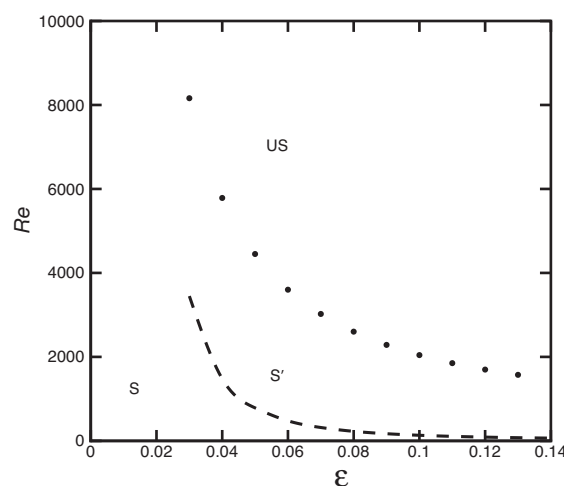

Fig. 2. Critical Reynolds number (upper curve) and the Reynolds number at which a vortex forms in the bulge (lower curve) versus ε for $\beta = 1$ and $m = 0$, where S indicates that the base flow is linearly stable with no vortex present in the bulge, S′ indicates that the base flow is linearly stable with a vortex present in the bulge, and US indicates that the base flow is linearly unstable.
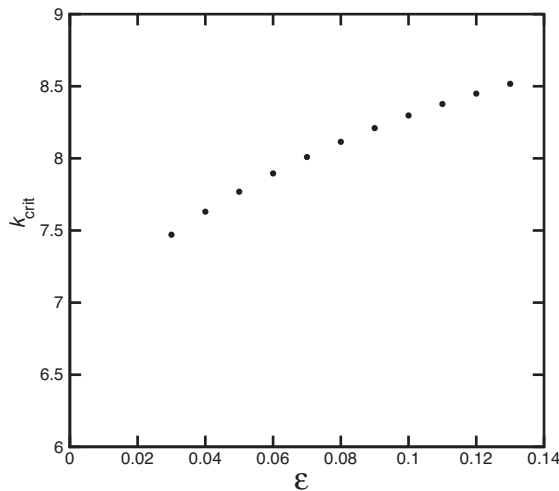
Fig. 3. Critical axial wavenumber versus ε for $\beta = 1$ and $m = 0$, where the corrugation wavenumber is 2π.

Fig. 4. Inverse critical Reynolds number versus ε for $\beta = 1$ and $m = 0$.

0 disturbances, but this value does not represent the global minimum. Furthermore, as ε decreases, the critical axial wavenumber seems to be decreasing toward the corrugation wavenumber (2π), as expected (see Fig. 3).

Because we are primarily interested in the small amplitude limit, we have only performed a cursory investigation into the effects of nonaxisymmetric disturbances (i.e., $m \neq 0$) to show that only axisymmetric disturbances need be considered in this limit. Thus, results show that the critical azimuthal wavenumber depends strongly on the value of ε and that $m_{crit} = 2$ for $0.16 \leq \varepsilon \leq 0.2$, $m_{crit} = 1$ for $0.1 < \varepsilon < 0.16$, and $m_{crit} = 0$ for $\varepsilon \leq 0.1$. For example, for $\varepsilon = 0.2$ the difference between the second transition Reynolds number (i.e., Re_{crit}) for $m = 2$ and $m = 0$ is $\approx 14\%$.

As shown in Fig. 2, the critical Reynolds number is a very strong function of ε, increasing rapidly with decreasing amplitude and suggesting the presence of a nonzero value of ε below which the base flow is linearly stable for all Reynolds numbers. As can be seen in Fig. 4, for small corrugation amplitudes, $1/Re_{crit}$ varies nearly linearly with ε. Extrapolation of a linear least-squares fit to the ε dependence of $1/Re_{crit}$ for the four and five smallest values of ε for which the critical Reynolds number was computed gives $\varepsilon^* \approx 0.006$, while extrapolation by quadratic least-squares for the four and five smallest values of ε gives $\varepsilon^* \approx 0.005$. On the other hand, extrapolation of a nonlinear least-squares fit of the form $Re = a(\varepsilon - \varepsilon^*)^b$ to all of the data gives
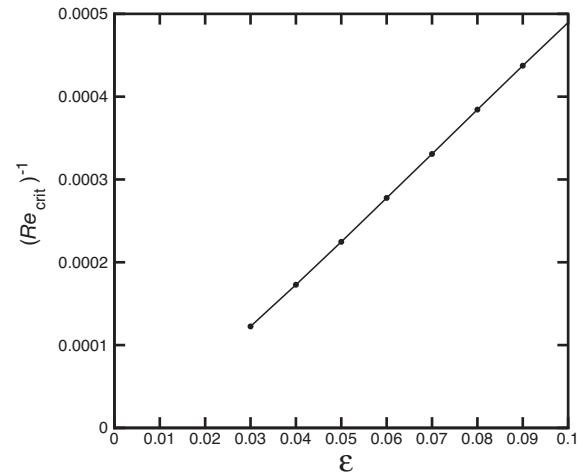
$\varepsilon^* \approx 0.006$, where the exponent b is approximately -1. We note that varying which subset of points is used in the extrapolation does not significantly change the linear and quadratic results, although for the nonlinear fit, one does see some variation.

In summary, these results suggest that for the rather large wall distortion (having a wavelength of the same order as the pipe diameter) investigated so far, the critical amplitude below which the base flow is linearly stable is somewhere around 0.006. Thus, below this amplitude, the current linear stability results are consistent with those for a smooth-walled pipe, where the flow is also linearly stable for all Reynolds numbers. This critical amplitude also seems to be close or nearly identical to the value below which no vortex forms in the bulge region at low Reynolds number. This suggests that the instability is directly tied to the formation of a vortex in the bulge region and that when the vortex cannot form, the flow is stable to infinitesimal disturbances, but that when it does form, the cause of the instability is likely to be vortex separation. In an attempt to understand the cause of the instability, critical conditions are recomputed after eliminating terms from the disturbance equations, and results show that fluctuations in the radial velocity component created as a result of the coupling between the radial derivative of the base flow axial velocity component and the radial perturbation velocity component lead to significant destabilization.

1. Reynolds O (1883) *Philos Trans R Soc London* 174:935–982.
2. Lessen M, Sadler SG, Liu TY (1968) *Phys Fluids* 11:1404–1409.
3. Davey A, Drazin PG (1969) *J Fluid Mech* 36:209–218.
4. Garg VK, Rouleau WT (1972) *J Fluid Mech* 54:113–127.
5. Barenblatt G, II, Chorin AJ, Prostokishin VM (1997) *Proc Natl Acad Sci USA* 94:773–776.
6. Herron IH (1991) *Phys Fluids* 3:1825–1827.
7. Salwen H, Cotton FW, Grosch CE (1980) *J Fluid Mech* 98:273–284.
8. Meseguer A, Trefethen LN (2003) *J Comput Phys* 186:178–197.
9. Deiber JA, Schowalter WR (1979) *AIChE J* 25:638–645.
10. Sobey IJ (1980) *J Fluid Mech* 96:1–26.
11. Stephanoff KD, Sobey IJ, Bellhouse BJ (1980) *J Fluid Mech* 96:27–32.
12. Deane AE, Kevrekidis IG, Karniadakis GE, Orszag SA (1991) *Phys Fluids A* 3:2337–2354.
13. Ghaddar N, El-Hajj A (2000) *Heat Transfer Eng* 21:35–46.
14. Nishimura T, Bian YN, Matsumoto Y, Kunitsugu K (2003) *Heat Mass Transfer* 39:239–248.
15. Mahmud S, Islam AKMS, Feroz CM (2003) *Heat Mass Transfer* 39:387–393.
16. Ghaddar NK, Korczak KZ, Mikic BB, Patera AT (1986) *J Fluid Mech* 163:99–127.
17. Cho KJ, Kim M, Shin HD (1998) *Fluid Dyn Res* 23:349–370.
18. Cabal A, Szumbarski J, Floryan JM (2002) *J Fluid Mech* 457:191–212.
19. Adachi T, Uehara H (2003) *Int J Numer Methods Fluids* 41:601–613.
20. Floryan JM (2003) *J Fluid Mech* 482:17–50.
21. Floryan JM (2005) *Phys Fluids* 17:044101.
22. Lahbabi A, Chang H (1986) *Chem Eng Sci* 41:2487–2505.
23. Reddy JN, Gartling DK (1994) *The Finite Element Method in Heat Transfer and Fluid Dynamics* (CRC, Boca Raton, FL).
24. Chen JH, Pritchard WG, Tavener SJ (1995) *J Fluid Mech* 284:23–41.
25. Goodwin RT, Schowalter WR (1996) *J Fluid Mech* 313:55–82.
26. Coddington EA, Levinson N (1965) *Theory of Ordinary Differential Equations* (McGraw–Hill, New York).
27. Cotrell DL, Pearlstein AJ (2004) *J Fluid Mech* 509:331–351.
28. Jeong J, Hussain F (1995) *J Fluid Mech* 285:69–94.

Corrections and Retraction

CORRECTIONS

INAUGURAL ARTICLE, GEOPHYSICS. For the article "Gravitational dynamos and the low-frequency geomagnetic secular variation," by P. Olson, which appeared in issue 51, December 18, 2007, of *Proc Natl Acad Sci USA* (104:20159–20166; first published November 29, 2007; 10.1073/pnas.0709081104), the author notes that on page 20160, left column, last paragraph, line 9, "then $\varepsilon = -1$ in Eq. **3**" should instead read: "use $\varepsilon = -1/\sqrt{4\pi}$ in Eq. **3**." This error does not affect the conclusions of the article.

APPLIED PHYSICAL SCIENCES. For the article "Instability in pipe flow," by D. L. Cotrell, G. B. McFadden, and B. J. Alder, which appeared in issue 2, January 15, 2008, of *Proc Natl Acad Sci USA* (105:428–430; first published January 4, 2008; 10.1073/pnas.0709172104), due to a printer's error, the year of publication appeared incorrectly in the footer. The correct publication date is "January 15, 2008." The online version has been corrected.

BIOCHEMISTRY. For the article "The globular tail domain puts on the brake to stop the ATPase cycle of myosin Va," by Xiang-dong Li, Hyun Suk Jung, Qizhi Wang, Reiko Ikebe, Roger Craig, and Mitsuo Ikebe, which appeared in issue 4, January 29, 2008, of *Proc Natl Acad Sci USA* (105:1140–1145; first published January 23, 2008; 10.1073/pnas.0709741105), the authors note that, due to a printer's error, ref. 25 contained an incorrect volume number. The corrected reference appears below.

25. Burgess SA, Yu S, Walker ML, Hawkins RJ, Chalovich JM, Knight PJ (2007) *J Mol Biol* 372:1165–1178.

DEVELOPMENTAL BIOLOGY. For the article "Linking pattern formation to cell-type specification: Dichaete and Ind directly repress *achaete* gene expression in the *Drosophila* CNS," by Guoyan Zhao, Grace Boekhoff-Falk, Beth A. Wilson, and James B. Skeath, which appeared in issue 10, March 6, 2007, of *Proc Natl Acad Sci USA* (104:3847–3852; first published February 26, 2007; 10.1073/pnas.0611700104), the authors note the following: "On page 3851, right column, first paragraph, line 9, in the sentence 'For example, Sox1 can bind directly to the *HES1* promoter and suppress its transcription (24, 32),' the references were cited in error. The correct reference is Kan L, Israsena N, Zhang Z, Hu M, Zhao LR, Jalali A, Sahni V, Kessler JA (2004) *Dev Biol* 269:580–594. Additionally, please note that ref. 24 is a duplicate of ref. 10. Finally, ref. 4 was cited in error on page 3852, left column, paragraph 3, line 4, and right column, paragraph 2, line 1, and should be removed from both locations. We apologize for any confusion these errors may have caused."

RETRACTION

PLANT BIOLOGY. For the article "*Arabidopsis* myosin XI mutant is defective in organelle movement and polar auxin transport," by Carola Holweg and Peter Nick, which appeared in issue 28, July 13, 2004, of *Proc Natl Acad Sci USA* (101:10488–10493; first published July 6, 2004; 10.1073/pnas.0403155101), the authors wish to note the following: "We must retract the results published in the article. In further investigations of the *mya2-1* knockout (SAIL_414_C04), we detected a second deletion upstream and adjacent to the *MYA2* locus, and a complementation assay performed with the whole genomic sequence of *MYA2*, including the promoter (10.5 kb), revealed no significant differences between the dwarf phenotype of the original mutant line and the *mya2*-rescued line. The analysis included parameters such as shoot length, cytoplasmic streaming, hypocotyl length, epidermal cell length, and root hair length. Therefore, the phenotype of the original knockout line was probably due to the second deletion upstream of the *MYA2* gene. Since our original publication, and consistent with our new results, others have observed no major defects resulting from inactivation of any of the 13 myosin XI genes in the *Arabidopsis thaliana* genome (1–3); inactivation of the *MYA2* and *XI-K* genes resulted only in defects in root hair growth and organelle trafficking (2, 3)."

Carola Holweg
Peter Nick

1. Hashimoto K, *et al.* (2005) Peroxisomal localization of myosin XI isoform in *Arabidopsis thaliana*. *Plant Cell Physiol* 46:782–789.
2. Ojangu EL, Järve K, Paves H, Truve E (2007) *Arabidopsis thaliana* myosin XIK is involved in root hair as well as trichome morphogenesis on stems and leaves. *Protoplasma* 230:193–202.
3. Peremyslov VV, Prokhnevsky AI, Avisar D, Dolja VV (2008) Two class XI myosins function in organelle trafficking and root hair development in *Arabidopsis thaliana*. *Plant Physiol*, 10.1104/pp.107.113654.